J Mater Sci (2008) 43:2947–2954
DOI 10.1007/s10853-007-1796-2

Protective coating for magnesium alloy

A. Abdel Aal

Received: 22 February 2007 / Accepted: 23 April 2007 / Published online: 3 July 2007

Abstract A phosphate–permanganate conversion coating was applied as the pretreatment process for AZ91D magnesium alloy substrate. Zn–Ni alloys were electrodeposited onto the treated AZ91D magnesium alloy from sulfate bath. The morphology and phase composition of the coatings were determined with X-ray diffraction (XRD) and Scanning Electron Microscope (SEM). The results reveal that the conversion rate depends on pH of solution and treatment time. Salt spray and the electrochemical polarization testing were applied to evaluate the corrosion performance of phosphate–permanganate and Zn–Ni coated alloys. It was found that Ni content in deposit is a function of current density and bath composition. Zn–13 wt.% Ni coating provides very good corrosion protective function to inner AZ91D magnesium alloy. Phosphate–permanganate treatment enhances the corrosion resistance of Zn–Ni coatings.

Introduction

Magnesium is the lightest of all metals used as the base for constructional alloys. Mg alloy is presently used in a wide range of structural applications such as aerospace, automotive, electronics and other industries. It is expected that applications, in particular involving motion or portability of the component, will increase in the future because of the material's high strength-to-weight ratio and a relatively high stiffness. However, magnesium is intrinsically highly reactive and its alloys usually have relatively poor corrosion resistance, which is actually one of the main obstacles to the application of magnesium alloys [1, 2].

However, being a highly chemically active alloy, plating on magnesium alloys needs special bath formulation and pretreatments. Hence, direct plating of magnesium is still a challenge for producers and researchers. The process becomes more complicated on AZ91D Mg alloy due to the microstructure heterogeneity owing to the uneven distribution of Al in the three constituent phases, which often leads to the non-uniform coating growth. In order for a coating to provide adequate protection, the coating must be uniform, well adhered and pore-free [3].

Common processes used to enhance corrosion resistance include physical surface medication, chemical conversion, electrochemical anodizing, chemical and electro-plating and organic coatings. Of these techniques, anodizing treatment is one of the most promising methods for magnesium alloys. These processes enhance certain properties including corrosion and/or wear resistance. The additional costs, however, often dictate the use for particular applications [4–8].

Chromate conversion coatings (CCCs) have been subjected to intensive study over the past decades due to the effective corrosion protection they confer to Al and Mg alloys and the desire to develop an effective and environment-friendly replacement. CCC is a corrosion protective coating system used on Al aircraft alloys. CCC is self-healing so that it continues to protect even when scratched [9]. The composition and structure of CCCs formed on pure Al and Al alloys have been extensively investigated by Frankel et al. using a variety of analytical tools such as scanning electron microscopy, focused ion beam sectioning

A. Abdel Aal (✉)
Surface Protection & Corrosion Control Lab, Central Metallurgical Research & Development Institute, CMRDI, P.O. 87, Helwan, Cairo, Egypt
e-mail: foralsayed@gmail.com

and scanning transmission electron microscopy with nanoelectron dispersive spectroscopy line profiling [9]. Chemical surface treatments, which have proven to effectively improve the corrosion resistance of magnesium alloys, include anodizing treatments and CCC treatments. However, the major component used in those treatments and processing baths, hexavalent chromium (Cr^{6+}), is an irritant and is caustic to skin and mucous membranes. Due to the environmental impact of hexavalent chromate and the imminence of associated restrictions, there is a great need for less harmful treatment methods [10].

Zinc alloy deposition has been of interest recently since such alloys provide better corrosion protection than unalloyed zinc coatings. Compared to conventional corrosion preventive coatings of magnesium alloys, Zn–Ni coatings are likely to have better anti-corrosion properties, especially when they have a Ni content of 12–14 wt.% and an intermetallic phase, viz γ-$Zn_{21}Ni_5$. The corrosion resistance of Zn–Ni coatings can be further improved by the chromating treatment. Therefore, if feasible technologies can be developed to create Zn–Ni coatings on magnesium alloys, the corrosion resistance of such alloys will be improved to a great extent [11–13].

For chromium-free conversion treatment of magnesium alloys, Hawke et al. studied the composition and performance of phosphate conversion coating [14]. Chong et al. investigated phosphate–permanganate conversion coating [15]. However, the researches on chromium-free conversion treatment mainly concentrated on compositions and structure of the coatings. Though there were scientists such as Gonzalez et al. who investigated the growth and formation of stannate conversion coating primarily [16].

The aim of the present work is to deposit Zn–Ni alloys onto AZ91D magnesium alloy using electrodeposition technique. Prior to Zn–Ni depositing, AZ91D substrate was immersed in a Zn^{2+}-containing solution and then treated with phosphate–permanganate solution to ease the cohesion process by raising the electric potential of the sample and improving the cohesion properties of Zn–Ni coatings.

Experimental

A commercial magnesium alloy AZ91D was used in this study as substrate. Figure 1 shows the microstructure of as-cast AZ91D Mg alloy. It is clear that, the AZ91D alloy consisted of primary α-Mg grains surrounded by a eutectic mixture of α and β-$Mg_{17}Al_{12}$ [17].

The preparation of the specimens includes mechanical polishing and cleaning in acetone by means of ultrasonic bath. Before depositing Zn–Ni alloys, the substrate surfaces were successively treated by following processes:

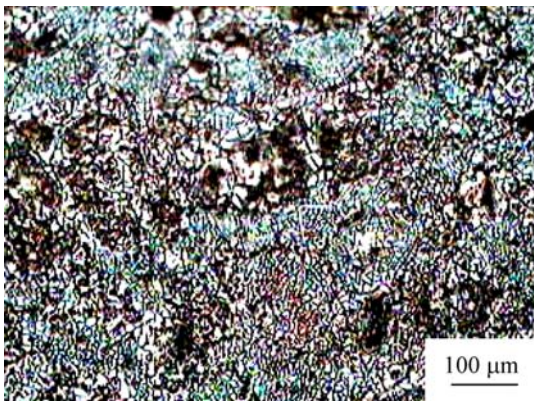

Fig. 1 Microstructure of as-cast AZ91D Mg alloy

1. Polishing with 380# alumina sand paper;
2. Alkaline cleaning in a solution containing sodium carbonate (Na_2CO_3), 20 g/L and tri sodium orthophosphate ($Na_3PO_4 \cdot 12H_2O$), 25 g/L operating at 60 ± 5 °C for 2–3 min;
3. Chemical pickling in a solution of 75% phosphoric acid operating at room temperature for 1 min;
4. Surface activation in a solution of 46% hydrofluoric acid operating at room temperature for 30 s;
5. Zincating by immersion with agitation for 1 min in a solution containing zinc oxide, sodium hydroxide ferric chloride and potassium sodium tartrate;
6. Conversion coatings were formed by immersing specimen in a phosphate–permanganate bath within pH 3–6;
7. Electrodeposition of Zn–Ni alloys was carried out from alkaline bath by mixing two aqueous solutions, i.e. a caustic solution containing Zn and a triethanolamine solution containing Ni. pH value of the mixed solutions was controlled to be above 12. The solution was stirred by magnetic stirrer (150 rpm) during the deposition and the electrodeposition process was carried out for 30 min;
8. Stripping the Zn–Ni alloy deposition using 10% HCl solution. The dissolved metal (Zn and Ni) was determined by atomic absorption technique using Perkin–Elmer, Atomic Absorption Model, A Analyst 200).

The composition of zincate, phosphate–permanganate and Zn–Ni baths are shown in Table 1.

Surface morphology of as-received Mg alloy, conversion coated samples and Zn–Ni coated material was examined with scanning electron microscope (JEOL-JSM-5410). The deposited films were analyzed using an X-ray diffractometer (BRUKER axc-D8) using Cu-K_α radiation with $\lambda = 0.1542$ nm. The cross-sectional microstructures of the coated samples were studied by Hotstage microscope (Olympus microscope provided with linkam software). The

Table 1 The composition of zincate, phosphate–permanganate and Zn–Ni baths

Bath compositions	Concentration (g/L)
Phosphate–permanganate bath	
$KMnO_4$,	40
K_2HPO_4	150
H_3PO_4	To maintain pH 3–6,
Zn–Ni bath	
Nickel sulfate	5–25
Zinc oxide	10
Sodium hydroxide	150
Triethanolamine	50
Zincate solution	
Sodium hydroxide	525
Zinc oxide	100
Ferric chloride	10
Potassium sodium tartrate	1

coating thickness was measured by Digital coating thickness gage (PosiTector® 6000).

Electrochemical polarization tests were performed in a corrosion cell that contained 250 mL of 3.5 wt.% NaCl solution at room temperature with a scan rate of 0.5 mV s^{-1}. All electrochemical measurements were carried out using an AUTOLAB PGSTATE 30 potentiostat/galvanostat and its M352 software. Platinum gauze was used as a counter electrode and silver/silver chloride (Ag/AgCl) was the reference electrode. The exposed area was 1 cm^2.

An ASTM B117 [18] salt spray test was undertaken to evaluate the corrosion performance of samples with and without coatings. The samples were kept in a chamber with salt spray at 35 °C. An aqueous solution of 5 wt.% NaCl was used for the tests.

Results and discussion

Phosphate–permanganate conversion coating

Figure 2 shows the morphology of the layer formed in the chemical conversion treatment using the phosphate–permanganate bath. Mud-cracks are clearly distributed allover the surface of conversion-coated layer. Such cracks can be attributed to hydrogen being released via the chemical reaction during the conversion treatment and/or the dehydration of the surface layer after treatment [15]. The hydrogen evolution can be explained on the basis of the reaction of phosphoric acid with Mg as follow:

$$6H^+ + 2PO_4^{3-} + Mg \longrightarrow Mg(H_2PO_4)_2 + H_2 \quad (1)$$

According to this reaction, hydrogen can be released at the cathode with the dissolving of anode [19]. Local cell

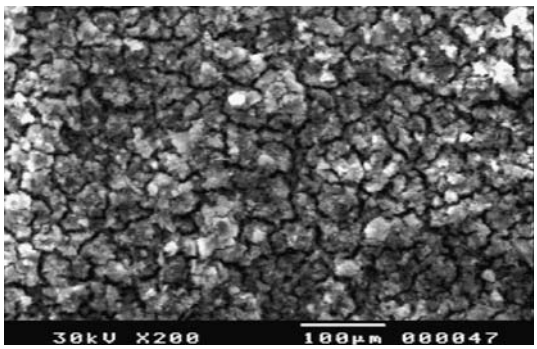

Fig. 2 SEM image of conversion coated AZ91D Mg alloy (treatment time: 10 min, pH: 4)

effects can be formed between the grain boundary acting as a cathode and grain functions as an anode forming. With reaction, hydrogen is released persistently and the products will gradually cover the grains. The concurrent development of hydrogen release and the reactants covering the surface forms the notches creating mud cracks as shown in Fig. 2. Cracks formation also can be attributed to the dehydration of the upper coating layer, which contains hydrated hydroxides such us $Mg(OH)\cdot xH_2O$ and $Al(OH)_3\cdot xH_2O$. Meanwhile, pH value is raised due to phosphoric acid (or H^+) being consumed at the interface of base metal and solution [15].

The variation of conversion coating thickness with immersion time and pH of solution were demonstrated in Fig. 3a,b. It is clear that the coating thickness increases with time up to 10 min. Further immersion time (10–14 min) has very low effect on conversion coating thickness. As the surface layer grows with increasing duration of immersion, visible cracks seen frequently in the chemical conversion surface layer become pronounced. According to Fig. 3b, the conversion-coating thickness decreased gradually with the increase of pH value. Practically, an incompact surface layer was formed if pH value of treatment bath was below 3.0. On the other hand, the speed of conversion reaction is quite slow during coating formation if pH value of treatment bath is above 5.0. Similar results have been obtained earlier by Zhao et al. [20].

The typical results of XRD analysis of AZ91D substrate as-received and conversion treated specimens by the phosphate–permanganate bath are shown in Fig. 4a,b. XRD spectra for substrate show peaks of base metal of Mg and $Mg_{17}Al_{12}$. However, XRD profile of the coated specimen was composed of magnesium aluminium oxide ($Mg_{0.36}Al_{2.44}O_4$), spinel ($MgAl_2O_4$), potassium manganese oxide ($K_2Mn_2O_3$) and phosphate products like Natrophilite ($NaMnPO_4$). The reasons for the formation of these oxides are explained elsewhere [21, 22] as follows:

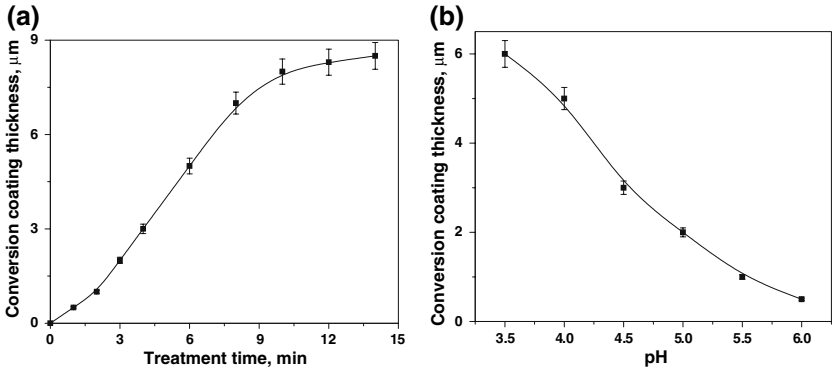

Fig. 3 The variation of conversion coating thickness with (**a**) treatment time and (**b**) pH

a- Dissolution of Mg and Al in the pickling bath:

$$Mg \longrightarrow Mg^{+2} + 2e^{-} \quad (2)$$

$$Al \longrightarrow Al^{+3} + 3e^{-} \quad (3)$$

b- Formation of oxides in pickling

$$Mg^{2+} + O^{2-}_{(producedinpicklingsolution)} \longrightarrow MgO \quad (4)$$

$$2Al^{3+} + 3O^{2-}_{(producedinpicklingsolution)} \longrightarrow Al_2O_3 \quad (5)$$

$$MgO_{(s)} + Al_2O_3 \longrightarrow MgAl_2O_4 \quad (6)$$

Electrodeposition of Zn–Ni

The electrodeposition of Zn–Ni alloys can be classified as anomalous, where zinc, which is the less noble metal, deposits preferentially [23]. Codeposition of Zn and Ni is, however, not always anomalous since at low current densities, it is possible to obtain normal deposition, where Ni deposits preferentially to Zn. Therefore, there is a transitional current density that has to be reached in order to start anomalous codeposition [24]. The transitional current density generally depends upon many factors, such as the anion type present in the plating bath, temperature, the concentration of the more noble metal ions, the ratio of metal ions in the plating bath, electrode material, stirring, etc. [25]. To reduce number of variables, all the experimental work have been carried out under constant conditions.

Figure 5 shows the effect of the deposition current density and Ni concentration in bath on the wt.% of Ni content in the deposited alloy. It is clear that Ni content in the alloy deposition layer increases with the concentration of Ni in the bath. As far as the effect of the current density was concerned, however, Ni content in the deposition layer was depressed at higher current density. This means that an increase in the applied current favors the deposition of zinc, and thus a decrease in the amount of nickel in the coating [26].

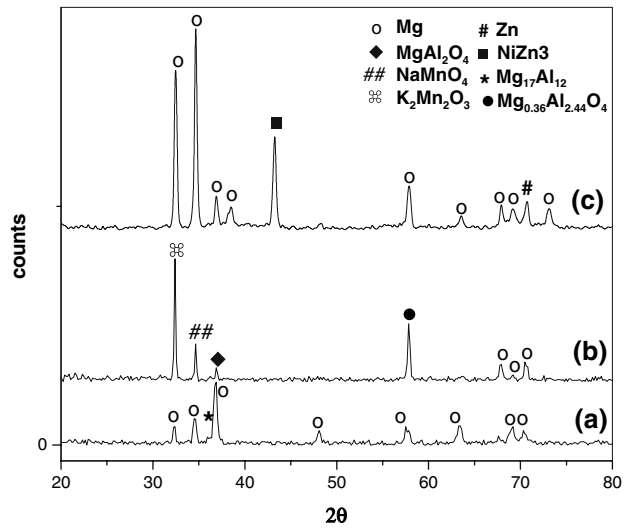

Fig. 4 XRD patterns of (**a**) as-cast, (**b**) conversion coated AZ91D Mg alloy and (**c**) coated with Zn–13 wt.% Ni alloy

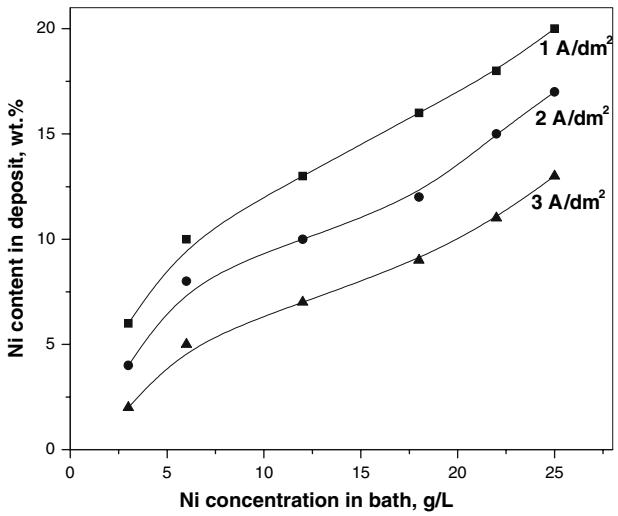

Fig. 5 Dependence of Ni content in deposit on Ni concentration in bath at different current densities

The influence of current density on the surface morphology of Zn–Ni alloys deposits is illustrated in Fig. 6(a–c). It is seen that an increase in current density resulted in increasing of particle size of the final deposit. At lower current densities (1–2 A/dm^2), smaller particles in the range 1–2 μm are observed while at higher current density (3 A/dm^2), particles exceeding 3–4 μm are seen. This is due to the preferred homogeneous nickel deposition at lower current densities and that of zinc at higher densities, which leads to agglomeration of particles resulting in larger particles [27].

An identification of phase structures present in the Zn–13 wt.% Ni alloy could be made on the basis of the chemical composition of the alloys, X-ray diffractogram (Fig. 4c) and equilibrium phase diagram of the binary Zn–Ni system [28]. Three strong and a few weak signals are observed and characterized for Zn and γ-phase (Ni_5Zn_{21}). As mentioned above, Zn–Ni alloys that contain 12–14 wt.% Ni can provide very good anti-corrosion properties [11–13]. Phase diagram shows that only γ-phase can be formed in this composition range, indicating that good corrosion resistance can be obtained if a Zn–Ni alloy merely consists of the γ-alloy [29]. Therefore, high corrosion resistance of the Zn–Ni coatings might primarily be attributed to the existence of the γ-phase [30].

Cross sectional view of the electrodeposited Zn–13 wt.% Ni alloys as obtained and after etching presented in Fig. 7. It was confirmed with optical microscopy that a layer of ~ 10 μm in thickness has been deposited on the surface of the Mg alloy substrate.

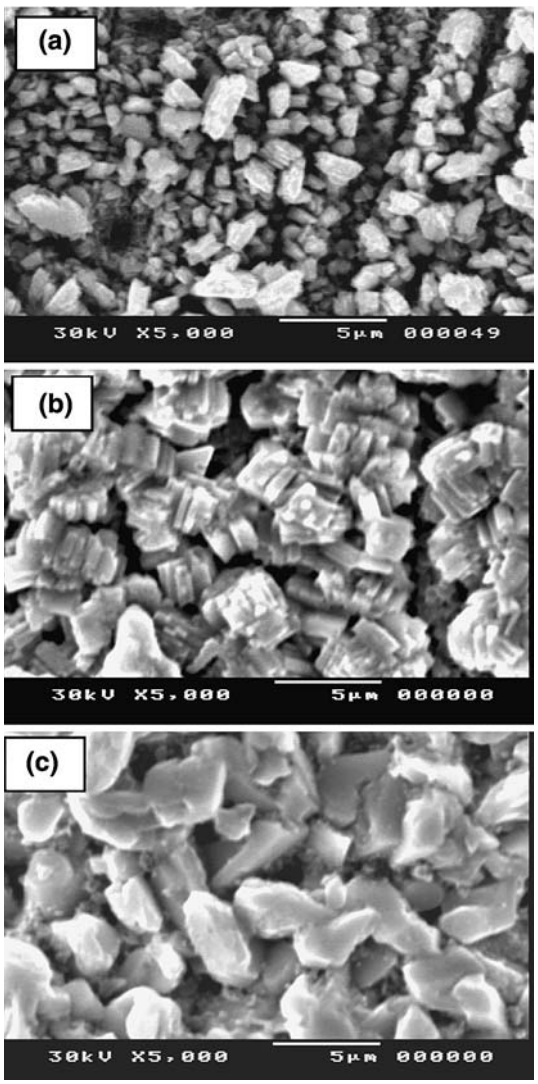

Fig. 6 SEM images of AZ91D Mg alloy coated with Zn–Ni using current density (**a**) 1 A/dm^2 (**b**) 2 A/dm^2 and (**c**) 3 A/dm^2

Corrosion measurements

Figure 8 shows the potentiodynamic polarization curves for the free substrate, phosphate–permanganate conversion coated layer and Zn–Ni alloys deposits respectively. The measurement was done in 3.5% NaCl solution at room temperature. The electrochemical parameters such as polarization resistance (R_p) were measured using M352 software. Corrosion current density (I_{cor}) was measured using the linear polarization resistance technique and obtained as a function of R_p, with β_c as the cathodic and β_a the anodic Tafel slopes that were obtained from polarization curves.

$$I_{corr} = \frac{\beta}{R_p} \quad \text{(I)}$$

where β is a constant value and can be calculated by following equation:

$$\beta = \frac{\beta_c \beta_a}{2.3(\beta_c + \beta_a)} \quad \text{(II)}$$

The values of β_c and β_a for Mg alloy are 0.037 and 0.091 V/dec, while for Zn–Ni deposit are 0.1 and

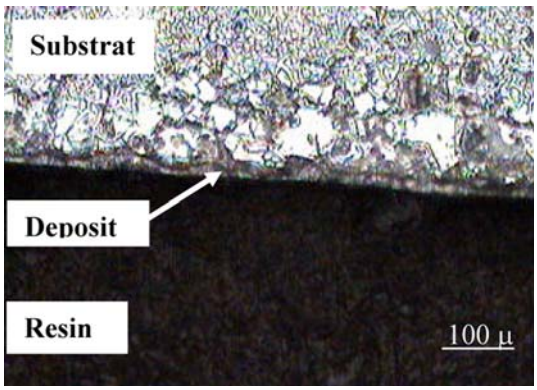

Fig. 7 The cross-sectional microstructure of the AZ91 Mg alloy with electrodeposited Zn–13 wt.% Ni

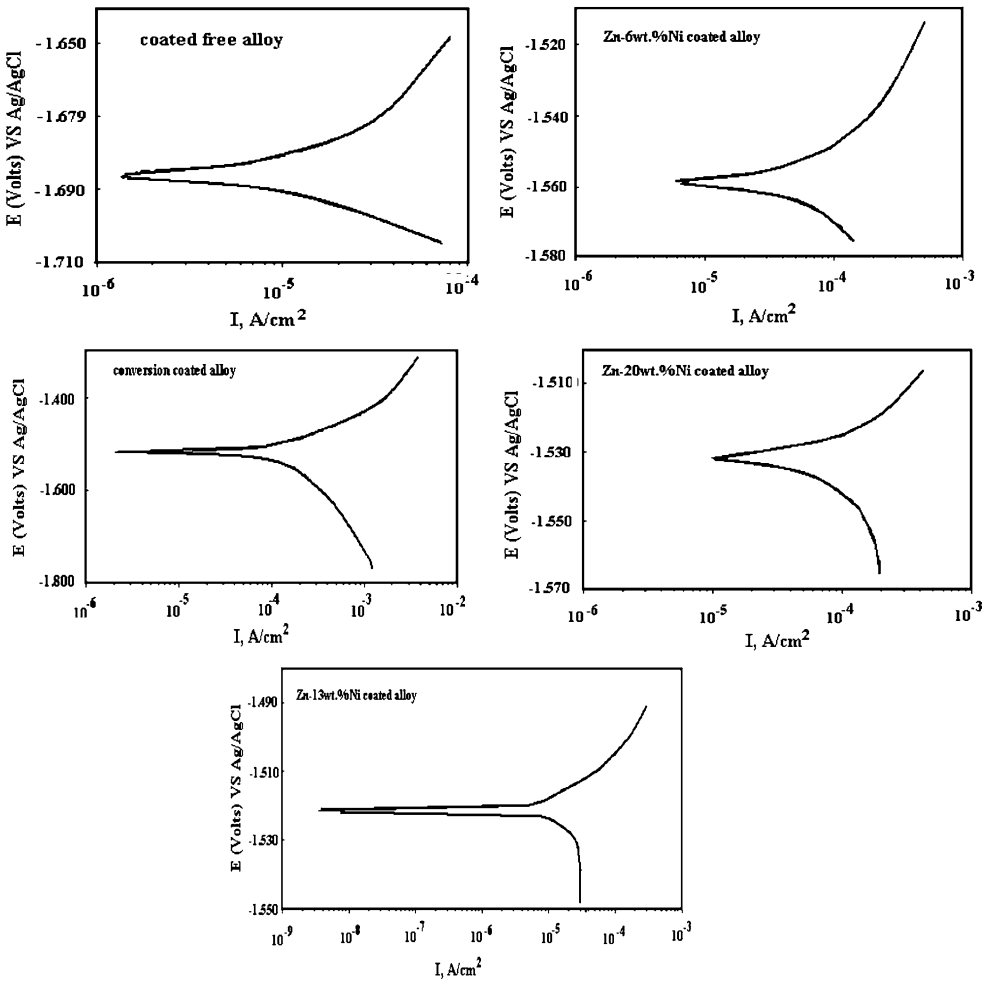

Fig. 8 The polarization curves for (**a**) as-cast AZ91D Mg alloy and the samples coated with (**b**) phosphate–permanganate and Zn–Ni coatings containing (**c**) 6 wt.%, (**d**) 20 wt.% and (**e**) 13 wt.% Ni

0.03 V/dec and for phosphate–permanganate 0.057 and 0.018 V/dec respectively. The corrosion rate, CR (expressed in mil per year), was obtained from I_{cor} according to the equation below:

$$\mathrm{CR(mpy)} = \frac{0.13 I_{\mathrm{Corr}}\,(\mathrm{eq.wt.})}{\rho} \qquad \text{(III)}$$

where eq. wt. is the equivalent weight and ρ is density in g/cm^3 and I_{cor} is the corrosion current density determined by the linear polarization method using the Stern-Geary equation [31].

The linear polarization resistance (R_p) and the Tafel characteristics of conversion coated and deposited Zn–Ni alloys is presented in Table 2. It is obvious that the deposit with 13 wt.% Ni shows the highest polarization resistance of 398 Ω/cm^2 because of the better barrier properties offered by nickel. The alloy composition with Zn–20 wt.% Ni measured a polarization resistance of 321 Ω/cm^2. Tafel polarization behavior shown in Fig. 8 indicates that the corrosion current is smaller for the deposited Zn–13 wt.% Ni as compared to the Zn–6 wt.% Ni and Zn–20 wt.% Ni alloys. Therefore, Zn–13 wt.% Ni alloys showed lower corrosion rates of 34.51 mpy when compared to the deposited Zn–6 wt.% Ni and Zn–20 wt.% Ni alloys that exhibited a corrosion rate of 44.63 and 42.84 mpy respectively (Fig. 9). This clearly indicates that increasing of zinc amount in the alloy leads to more sacrificial property and the deposit with low zinc and high nickel contents offers more barrier property towards corrosion protection.

The percent protection efficiency values (E%) and the porosity values (P%) in coatings were estimated using below equations, respectively [32–34] :

$$\mathrm{E\%} = \frac{R_P^{-1}(\mathrm{uncoated}) - R_p^{-1}(\mathrm{coated})}{R_P^{-1}(\mathrm{uncoated})} \times 100 \qquad \text{(IV)}$$

$$\mathrm{P\%} = \left[\frac{R_P(\mathrm{uncoated})}{R_P(\mathrm{coated})}\right] \times 10^{\left(\frac{-|\Delta E_{\mathrm{Corr}}|}{\beta_a}\right)} \times 100 \qquad \text{(V)}$$

where ΔE_{corr} is the difference between corrosion potentials and β_a is anodic tafel slop for steel substrates that was

Table 2 Electrochemical corrosion data related to polarization curves of as-cast AZ91D Mg alloy and coated samples

Sample composition	R_p, Ω /cm^2	I_{cor}, A/cm^2	E_{cor}, V	CR, mpy	P, %	E, %
Coat-free alloy	47	5.6×10^{-4}	–1.685	502.10	–	–
Phosphate–permanganate	270	5.1×10^{-5}	–1.635	46.80	9.2	82.6
Zn–6 wt.% Ni alloy	307	7.5×10^{-5}	–1.560	44.63	5.8	84.7
Zn–13 % Ni alloy	398	5.8×10^{-5}	–1.515	34.51	3.2	88.2
Zn–20% Ni alloy	321	7.2×10^{-5}	–1.585	42.84	6.7	85.4

obtained from the polarization curves. The results show that the corrosion resistance of Zn–13 wt.% Ni gives the best protection. This is in agreement with the results of the other researchers [35, 36].

During corrosion, zinc dissolves preferentially, leaving a top layer enriched with nickel. This layer acts as a barrier to further attack. The reason for higher corrosion resistance of Zn–13 wt.% Ni deposit compared with the Zn–6 and 20 wt.% Ni alloy coatings could be explained by the lowest of the porosity in this coating (3.2%) and its single γ-phase structure and hence the absence of local cells between different phases that would be present in the case of the dual phase coatings like Zn–13 wt.% Ni [36].

Salt spray testing was performed to evaluate the coating performance under accelerated corroding conditions in a salt spray test chamber whose temperature was set at 35 °C. The samples were exposed to a constant 5% salt fog in accordance with the ASTM B117 specifications [18]. The deposit thickness in all the cases was 10 μm. No post treatment or passivation was provided on the surface of the coatings. The samples were visually examined and the appearance of the white rust was observed as a function of time (Fig. 10). It can be noticed that phosphate–permanganate conversion treatment improves the corrosion resistance significantly. Therefore, it can be seen that the time to white rust formation increases with increasing wt.% of Ni content in deposit and the best protection is achieved by conversion treated alloy with Zn–13 wt.% Ni alloy coating. The corrosion of Zn–Ni layers in NaCl solution involve a series of reactions based on calculations of thermodynamic energy, as listed below [29]:

$$Zn + 2H_2O \longrightarrow Zn(OH)_2 + 2H^+ + 2e^- + 81.52\,kJ/mol \quad (6)$$

$$2Zn + 4H^+ + O_2 \longrightarrow 2Zn^{2+} + 2H_2O + 294.4\,kJ/mol \quad (7)$$

$$Zn(OH)_2 \longrightarrow ZnO + H_2O - 1.42\,kJ/mol \quad (8)$$

$$O_2 + 2H_2O + 4e^- \longrightarrow 4OH^{-1} + 158.74\,kJ/mol \quad (9)$$

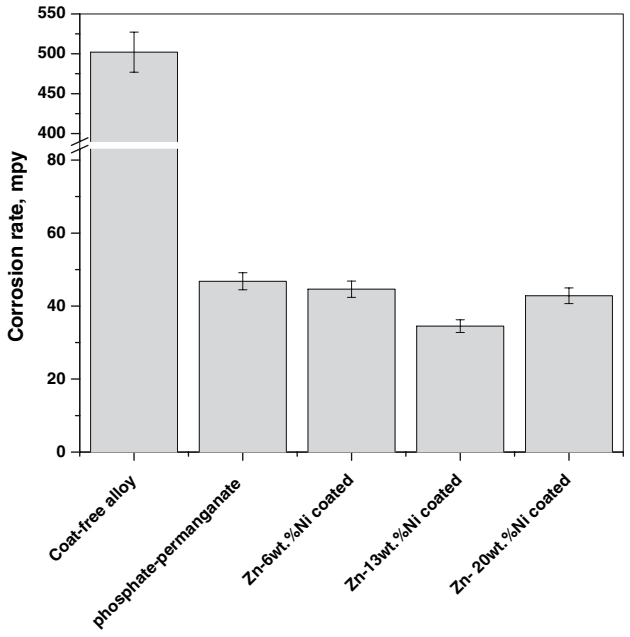

Fig. 9 The corrosion performance of the prepared samples

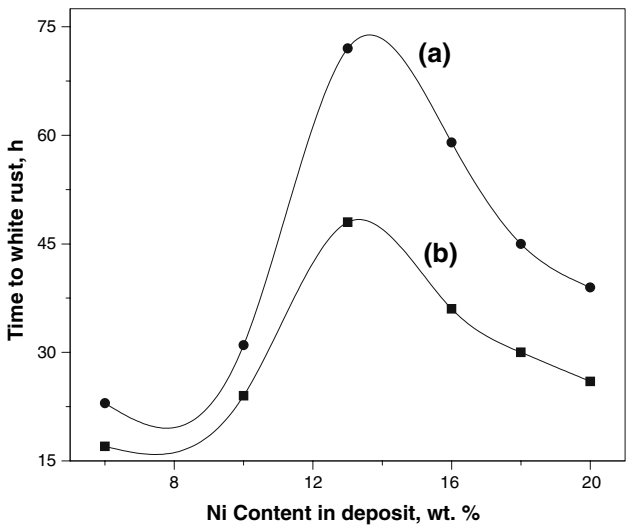

Fig. 10 Results of salt spray test for AZ91D Mg alloy coated by Zn–13% Ni (**a**) with and (**b**) without phosphate–permanganate pretreatment

$$5Zn^{2+} + 2O^{2-} + 2CO_2 + 6OH^{-1} \longrightarrow 2ZnCO_3 \cdot 3Zn(OH)_2 + 182.6\,kJ/mol \quad (10)$$

$$5Zn^{2+} + 2Cl^{-1} + 8OH^{-1} \longrightarrow ZnCl_2 \cdot 4Zn(OH)_2 + 328.5\,kJ/mol \quad (11)$$

Conclusions

A phosphate–permanganate conversion film was used as the pretreated layer Zn–Ni alloys on the AZ91D magnesium alloy substrate. The highest conversion rate is obtained from phosphate–permanganate solution of pH 3 and for 10 min treatment. The conversion-coated layer is crystalline and composed of magnesium aluminum oxide ($Mg_{0.36}Al_{2.44}O_4$), spinel ($MgAl_2O_4$), potassium manganese oxide ($K_2Mn_2O_3$) and phosphate products like Natrophilite ($NaMnPO_4$). Electrodeposition of Zn–Ni alloys has been performed onto the conversion treated alloy from the sulfate bath. Ni content in the deposited layer was depressed at high current density, where Zn deposition was predominant. The best deposit which meet a Ni content of 13 wt.% in the alloy layer, were obtained from electrolyte containing 20–25 g/L of $NiSO_4$ at 3 A/dm^2. The results of salt spray test and electrochemical potentiodynamic polarization experiment indicated the corrosion resistance of the coatings is the highest for Zn–13 wt.% Ni alloy due to the existence of γ-phase and the homogeneous and compact structure of the coatings.

References

1. Gray JE, Luan B (2002) J Alloys Compd 336:88
2. Shahin GE (2002) Minerals. metals and materials society, seattle, WA, United States, p 263
3. Ambat R, Zhou W (2004) Surf Coat Technol 179:124
4. Zozulin AJ, Bartak DE (1994) Met Finish 92:39
5. Khaselev O, Weiss D, Yahalom J (1999) J Electrochem Soc 146:1757
6. Khaselev O, Weiss D, Yahalom J (2001) Corros Sci 43:1295
7. Khaselev O, Yahalom J (1998) Corros Sci 40:1149
8. Liu Z, Gao W (2006) Surf Coat Technol 200:3553
9. Qingjiang M, Frankel GS (2004) Surf Interface Anal 36:30
10. Budavari S (1996) The merck index: An encyclopaedia of chemical, drugs and biologicals. 12th ed., Merck Research Laboratories, NJ, p 1475
11. Zaki N (1989) Met Finish 87:57
12. Sizelove RR (1991) Plat Surf Finish 78:26
13. Pushpavanam M, Natarajan SR, Balakrishan K, Sharma LR (1991) J Appl Electrochem 21:642
14. Hawke D, Albight DL (1995) Met Finish 10:34
15. Chong KZ, Shi TS (2003) Mater Chem Phys 80:192
16. Gonzalez-Nunez MA, Skeldon P, Thompson GE, Karimzadeh H (1999) Corrosion 55(12):1136
17. Ambat R, Zhou W (2004) Surf Coat Technol 179:124
18. ASTM B117 (2003) Standard test methods of salt spray testing. ASTM, Conshohocken, PA
19. Song G, Atrens A, Dargush M (1999) Corros Sci 41:249
20. Zhao M, Wu S, Luo J, Fukuda Y, Naka H (2006) Surf Coat Technol 200:5407
21. Moulder JF, Stickle WF, Sobol PE, Bomben KD (1995) In: Chastain J, King RC Jr (eds) Handbook of X-ray photoelectron spectroscopy - a reference book of standard spectra for indentification and interpretation of XPS Data. Physical Electronics Inc., Eden Prairie, MN
22. Gabis V, Ildefonse JP, Depussay B, Richard M, Stucky M (1997) Key Eng Mater 127:1653
23. Brenner A (1963) Electrodeposition of Alloys, vol 2. Academic Press, New York, p 194
24. Despic AR, Jovic VD (1995) In: Conway BE, White E, Bockris JOM (eds) Modern aspects of electrochemistry, vol. 27. Plenum Press, New York, p 54
25. Bajat JB, Stankovic VB (2004) Prog Organic Coatings 49:183
26. Lee HY, Kim SG (2000) Surf Coat Technol 135:69
27. Ganesan P, Kumaraguru SP, Popov BN (2006) Surf Coat Technol 201:3658
28. Porter DA, Easterling KA (1980) Phase transformations in metals and alloys. Van Nostrand Reinhold, Wokingham
29. Fratesi R, Roventi G (1996) Surf Coat Technol 82:158
30. Jiang F, Liu LF, Zhai CQ, Zhu YP, Ding WJ (2005) Thin Solid Films 484:232
31. Ozyilmaz AT, Kardas G, Erbil M, Yazici B (2005) Appl Surf Sci 242:97
32. Creus J, Mazille H, Idrissi H (2000) Surf Coat Technol 130:224
33. Patil S, Sainkar SR, Patil PP (2004) Appl Surf Sci 225:204
34. Bockris J, Reddy KN (1976) Modern electrochemistry, Plenum, New York, p 622
35. Sohi MH, Jalali M (2003) J Mater Proc Technol 138:63
36. Hall DE (1983) Plat Surf Finish 70:59